Journal of Molecular Liquids 340 (2021) 116898

Contents lists available at ScienceDirect

Journal of Molecular Liquids

journal homepage: www.elsevier.com/locate/molliq

Local molecular environment drives speciation and reactivity of ion complexes in concentrated salt solution

Nikhil Rampal [a,b], Hsiu-Wen Wang [a], Denys Biriukov [d,e], Alexander B. Brady [a], Joerg C. Neuefeind [c], Milan Předota [d], Andrew G. Stack [a,*]

[a] Chemical Sciences Division, Oak Ridge National Laboratory, Oak Ridge, TN 37831, USA
[b] Department of Chemical Engineering, Columbia University, New York, NY 10027, USA
[c] Neutron Scattering Division, Oak Ridge National Laboratory, Oak Ridge, TN 37831, USA
[d] Department of Physics, Faculty of Science, University of South Bohemia, České Budějovice 370 05, Czech Republic
[e] Institute of Organic Chemistry and Biochemistry, Czech Academy of Sciences, Prague 16610, Czech Republic

ARTICLE INFO

Article history:
Received 4 March 2021
Revised 11 June 2021
Accepted 30 June 2021
Available online 10 July 2021

Keywords:
Ion complexes
Concentrated aqueous solutions
Reaction mechanisms
Neutron diffraction
Rare event methods

ABSTRACT

The speciation and reactivity of aqueous salt solutions are important for a wide variety of applications. However, application of this information is inhibited by broad disagreement about composition, mechanisms, and structure in concentrated solutions especially. Here, neutron diffraction with isotopic substitution measurements on aqueous zinc chloride solutions are used to calibrate molecular dynamics simulations that include effective electronic polarization. This allows us to probe the origin of speciation and reactivity of zinc chloride-water ion complexes, $ZnCl_x(H_2O)_y^{2-x}$ ($x \leq 4$ and $y \leq 6$), by comparing the reactivity of species in concentrated (4.5 m) and dilute (0.01 m) conditions. Within the concentrated solution, it is found that the extended solvation environment is dominated by solvent-separated ion complexes whose presence increases the free energy of activation for interconversion of species while simultaneously enhancing their thermodynamic stability. This concentration-dependent reactivity and stability suggests that other reactions, such as the nucleation of solid phases, will also be affected.

1. Introduction

The extent of ion association in concentrated aqueous salt solutions is critically important to understand both equilibrium (e.g., speciation, activity-concentration relationships) and dynamic (e.g., viscosity, diffusivity, and conductivity) processes. Moreover, a consistent molecular picture that describes how associated ions form the precursors for the nucleation of solid phase(s) from solution is still missing [1–5]. Arguments for the mechanism(s) of nucleation as involving either simple ion-pairs or formation of complex hydrated networks or clusters of solute species remain highly debated [1,2,6–9]. The formation of ion complexes and the kinetics of association appear to be the key to resolve the chemical processes behind classical vs. non-classical nucleation [1,2,10,11]. A challenge in resolving this debate is that existing estimates of the equilibrium constants for ion association (K_A) found in thermodynamic speciation databases are often fit parameters rather than direct observations, derived after applying an activity-concentration relationship model [12–14]. Despite the practical usefulness of that approach, it loses the underlying atomic-scale chemistry necessary to understand reaction mechanisms. A more informative approach would be to consider ion complex formation through metal–ligand (ML) (inter)exchange processes (L = anions or water solvents) and incorporating the influence of extended solvation environments on the ligand exchange reactions [15–19]. However, it is not well understood how specific solvation environments influence ion association reactions at this time. Especially at high salt concentrations, the role of water/solvents is poorly understood but is also simultaneously integral to determining reaction mechanisms. Thus, the precise nature of the solvation environment at the molecular scale is expected to affect the reactivity of the solution (e.g., due to ion aggregation), control transport properties (e.g., increase of viscosity, decrease of diffusivity and mobility) and drive reaction outcomes (e.g., precipitation mechanisms and phase selection).

In principle, atomic-scale simulations could deliver the mechanistic and atomic-scale structural information necessary to resolve the molecular speciation of ion association. However, well known classical molecular dynamics models [20,21] used *as written* have

* Corresponding authors.
E-mail addresses: wanghswen@gmail.com (H.-W. Wang), stackag@ornl.gov (A.G. Stack).

https://doi.org/10.1016/j.molliq.2021.116898
0167-7322/

yielded poor agreement with the literature ion-pairing data [22], attributed to lack of explicit parameterization of ion interaction terms. In addition, our recent work suggests that the simple point charge models that contain formal charges on the dissolved ions may over-estimate the extent of ordering of the solvent and solutes bound to the ion [23,24]. As an alternative to classical models, *ab initio* computational models relieve the requirement for explicit parameterization of ion interaction but face a different challenge in that the time scales at which solutes equilibrate their solvation structures are sometimes slower [25] than the time-scales that can be practically simulated, even while using rare event methods. Given the difficulties in making experimental estimates, the reliability of computational models, and comparing these, it is therefore not surprising that there are conflicting interpretations of the stability of specific ion pairs/clusters.

In this Article, we show that a significant improvement in the solution structure can be achieved using high precision neutron diffraction isotope substitution (NDIS) measurements to tune electronic continuum correction molecular dynamics (ECC-MD) simulations. The role of the extended solution structure in determining the reactivity of associated ions is then probed using both direct simulation and a rare event method, well-tempered metadynamics [26,27], that allows us to discover and compare the reaction mechanisms and stability constants of ion association reactions in both concentrated and dilute solutions. The specific system we use is 4.5 m $ZnCl_2$ in water, and we find that interactions between aqueous Zn^{2+} with dissolved Cl^- and water molecules create a series of distinct coordination states, which can be recognized as local ion complexes: $ZnCl_x(H_2O)_y^{2-x}$ (where, x = 0–4 and y = 6–0). Interconversion of ion complexes occurs through barriers that are many multiples of k_BT in energy and the barriers for their interconversion increase in the concentrated solution. Reaction kinetics for interconversion are hindered, as compared to more dilute conditions, while the thermodynamic stabilities of the species are found to be concentration dependent. Specifically, the second-shell water molecules and/or third-shell solutes surrounding the as-formed ion complexes not only control the fluctuation in local atomic connectivity that influences reaction kinetics and mechanism, but also play an intimate role in changing the thermodynamic stability of the complexes, evidenced by the changing association constants for complex formation.

We chose to study the concentrated chloride solution paired with high charge density metal-cation (Zn^{2+}) in this work because (i) formation of ion complexes is established at concentrations above ~ 2 m [28–32], and (ii) it is possible to perform simultaneous manipulation of both $^{37}Cl/^{nat}Cl$ and $D/^{nat}H$ isotopes in the system which makes NDIS a unique approach that allows only Cl^--O_w solvation, Zn^{2+}-Cl^-, and Cl^--Cl^- correlations to be observed. Additionally, the extensive experimental and computational studies, which include multiple experimental measurements, have resulted in diverse and sometimes conflicting pictures of the chemical structure of associated species and thermodynamic speciation in $ZnCl_2$ solutions of similar concentration [28,30,32–34]. Specific issues include that speciation models disagree on relative proportions and types of ion complexes present (e.g., zinc tri- and tetrachloride, $ZnCl_3^-$ and $ZnCl_4^{2-}$) [28,30] and Pitzer activity coefficient models of $ZnCl_2$ solutions vary widely [35]. By combining and validating the ECC-MD simulations with experimental Cl-NDIS data, it has allowed us to achieve a clear picture of chemical speciation, equilibrium concentrations, association constants (K_A) for ion-pair formation, and quantifying the role of solvation structures in affecting reactivity. These lessons have implications for the key chemical processes relating to mineral nucleation, growth, and dissolution in complex aqueous solutions.

2. Materials and methods

2.1. NDIS and first-order difference analyses

A successful NDIS experiment depends first on obtaining two high-quality samples that are identical in all respects, except the isotope of one element has been changed. Secondly, a high-flux neutron source (e.g., accelerator-based neutron source) containing stable instrumentation is required, so that sufficient statistical accuracy and reproducibility in the data can be achieved. For the first factor, the chemical purity of the isotopically-labeled compounds largely determines the quality of prepared solutions. In this study, the source of ^{37}Cl is in the form of $Na^{37}Cl$ salt powders, produced from the Stable Isotope Production Program at Oak Ridge National Laboratory (ORNL). To extract ^{37}Cl from $Na^{37}Cl$ salts, cation exchange reactions using H^+ loaded resins (AG 50 W-X12, Dowex) were applied to convert dissolved $Na^{37}Cl$ to acidic $H^{37}Cl$ solution. Zn metal pellets (99.99%, 10440, Alfa Aesar) were then dissolved in excess $H^{37}Cl$ to produce aqueous solutions of $Zn^{37}Cl_2$. Preparation of 4.5 m $Zn^{37}Cl_2$ in null water requires additional purification steps, which include precipitation via evaporation and resuspension in null water. To maintain consistent concentration/isotope content, identical preparation procedures were applied to both isotopically labeled and naturally abundant samples. Detailed methods are given in Supplementary Material, Section S1. Confirmation of the synthesis method by X-ray diffraction and thermogravimetric Analysis-Mass Spectrometry is shown in the Supplementary Material, Section S2. Table 1 summarizes the stoichiometric composition of each prepared solution, along with estimated scattering errors caused by concentration imperfections.

Prepared solutions were sealed into quartz NMR tubes (507-PP-7QTZ, Wilmad-LabGlass) and loaded in the sample shifter carousel at the Nanoscale Ordered Materials Diffractometer (NOMAD) [36] instrument at the Spallation Neutron Source (SNS), ORNL. For each solution, scattering data were collected in 30 frames (30 mins. per frame) at room temperature for a total of 15 h at 60 Hz setting. The beamline's auto-reduction software [36] was used to normalize data and perform the NDIS first-order difference analyses. Details on data reduction and difference analyses are provided in Supplementary Material, Section S3. Briefly, the first-order difference approach comprises: (i) subtraction between two total structure factors F(q), from diffraction data involving Cl isotope substitutions (generating a ΔF_{Cl}), and (ii) Fourier transformation of the as-obtained ΔF_{Cl} intensities into the real-space signal, i.e., the first-order difference RDF $\Delta G_{Cl}(r)$.

2.2. Molecular dynamics simulations

Molecular Dynamics simulations were carried out using LAMMPS [37,38] and GROMACS [39–41] software packages in canonical (NVT) and isothermal-isobaric (NPT) ensembles [42].

Table 1
Isotopic compositions for pairs in $ZnCl_2$ solutions.

Solution pairs	NDIS difference
4.53(2)* m zinc chloride in null water	3 partial structural factors‡
4.51 m: $(Zn^{nat}Cl_2)_{1.0}(^nH_2O)_{12.306}$	Zn^{2+}-Cl^-, Cl^--O_w, Cl^--Cl^-
4.54 m: $(Zn^{37}Cl_2)_{1.0}(^nH_2O)_{12.225}$	

*At the target concentration of 4.5 m, the scattering contrast on the Cl substitutions is ~ 15.3 millibarns/sr/atom, i.e., ~33.6% of the total scattering. Thus, the concentration imperfections by 0.03 m will result in ~ 0.1% errors in the measured intensities.
‡ For regular neutron diffraction of $ZnCl_2$ in D_2O, a total of 10 partial structural factors is measured.

GROMACS was used for "unbiased/direct" simulations (on the microsecond time scales) and LAMMPS was used for well-tempered metadynamics [27] (WTM) "biased" simulations (see Supplementary Material, Section S5 for setup details). Results from both packages broadly agreed. The initial configurations were generated using Packmol [43] software with a tolerance of 2 Å. Classical "unbiased" simulations were run for 5 microseconds at 1 atm and 300 K with a timestep (ts) of 1 fs whereas "biased" simulations were run for 300 ns. Comparisons to the experimental RDF data were made following Wang et al.[23]. Briefly, the atomic or molecular pair-wise correlations are obtained from the average atom positions from the CMD simulations. These partial RDF's are then multiplied by their corresponding neutron-weighted scattering coefficients to produce RDFs in accord with experimental observations (for detail methods see Supplementary Material S4).

After initial attempts using a formal charge force field, an electrostatic continuum correction (ECC) model was used instead [31] (comparison is presented in Supplementary Material, Section S5.1). According to the ECC formalism, formal charge models overestimate electrostatic interactions since the polarization and screening effects innate to aqueous media are not accounted for [44], this can lead to more ordering in the primary solvation shell and the bulk structures than is observed experimentally (e.g., Supplementary Material, Figure S6 and our previous work [24]). Previous studies have focused primarily on the ion-pairing parameters, but that method did not consider the second-order (Cl^--Cl^- and Cl^--O_w) interactions [31]. To address this issue, the ECC model [31,44] here is implemented along with systematic changes to the Lennard-Jones parameters to fit the ECC-MD simulation RDF to the experimental Cl-NDIS data (see Supplementary Material, Section S5.1).

Potential of Mean Force (PMF) calculations were performed by well-tempered metadynamics using the PLUMED 2.5 [45] plugin with gaussian laid every 1000 timesteps, an initial height of 2.5 kJ/mol ($\approx 1\ k_BT$), and a bias factor of 8 (2D-PMF; Supplementary Material, Section S5.2) or 5 (1D-PMF; Supplementary Material, Section S5.3). Free energy surface calculations were performed in both concentrated (4.5 m) and dilute (0.01 m) conditions, and their comparison is displayed in Fig. 2 (for 2D-PMF) and Supplementary Material, Figures S8 and S9 (for 1D-PMF). Speciation analyses (Supplementary Material, Section S7) from unbiased simulations were calculated by counting specific species over a 500 ns windowed average. Separate speciation analyses were also performed from biased simulations by taking the Boltzmann distribution of the 2D-PMF using the program Metadynminer [46]. Identification of minimum energy paths for the interconversions of different species and reaction mechanisms, incorporating two different approaches (a nudge elastic band method and trajectory analysis) are detailed in Supplementary Material, Section S8. Equilibrium constants for ion association (K_A) reactions were calculated by taking the ratio of the integrals of the product and reactant states in the 1D-PMF (details in Supplementary Material, Section S9). Supplementary Material, Section S10 depicts the composition of multimer species and their propensity to occur at 4.5 m.

3. Results and discussion

3.1. NDIS with double isotopic substitutions and ECC-MD simulations

The nature and extent of contact ion-pairing and association were examined in concentrated aqueous solutions of zinc chloride, $ZnCl_2$. Labeled $Zn^{37}Cl_{2(s)}$ and naturally abundant $Zn^{nat}Cl_{2(s)}$ salts were created and purified to keep the preparation of the two samples consistent in all possible respects while minimizing contaminants. These two salts were dissolved in null water (^nH_2O = mixture of light and heavy water with a mole ratio of 0.64 H_2O:0.36 D_2O) to produce a pair of solutions that allow essentially a double isotopic labelling, chlorine atom and hydrogen on water (Table 1). The concept behind NDIS difference analysis is to measure the diffraction of a pair of solutions that are identical in all respects, except that the isotope of one of the elements (^{37}-Cl/^{nat}Cl) is distinct in each solution. By relying on the dependence of the neutron coherent scattering on the specific isotope, partial structure factors with respect to just the chlorine atoms can be obtained directly (Table 1). Details of the NDIS method are provided in Supplementary Material, Section S3, but in general are similar to those in our previous work [23]. In the final, normalized,

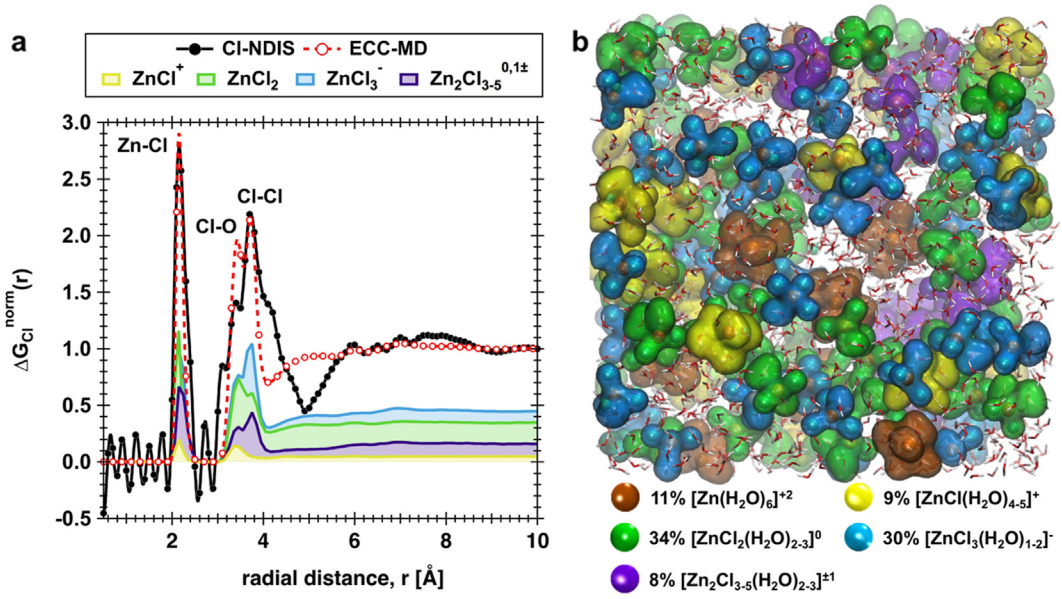

Fig. 1. Structure of 4.5 m $ZnCl_2$ aqueous solution, with comparison of experiment and simulation: **(a)** Comparison of normalized, Fourier-transformed RDF (ΔG_{cl}^{norm}) from neutron diffraction with isotope substitution, NDIS (black curve) to tuned ECC-MD simulations (dashed red curve with open circles). The tuned ECC-MD RDF is decomposed into its molecular RDFs (shaded colored curves) containing each molecular unit, $ZnCl^+$ (yellow), $ZnCl_2$ (green), $ZnCl_3^-$ (Blue) and $Zn_2Cl_{3\text{-}5}^{\pm1,0}$ (purple) present in 4.5 m $ZnCl_2$ solution. (b) Tuned ECC-MD simulation snapshot representing 4.5 m $ZnCl_2$ solution with its molecular species (van der Waals radius for each species is indicated with colored shells).

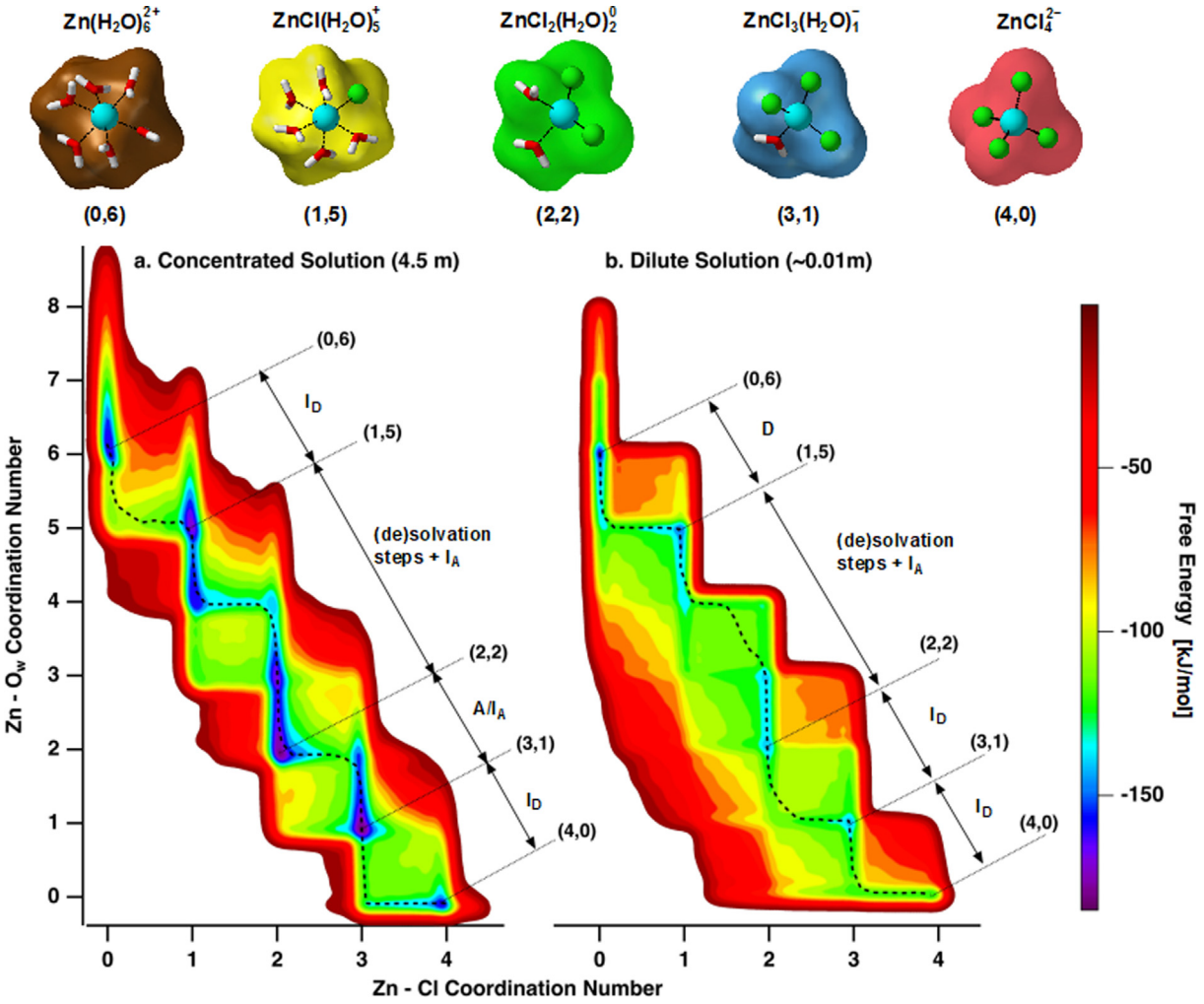

Fig. 2. Free energy surfaces using Zn-Cl and Zn-O_W coordination numbers as collective variables for concentrated (4.5 m) and dilute (0.01 m) $ZnCl_2$ solutions. The stable states (purple) along with the metastable states (dark blue) are connected by minimum energy paths (black dashed line) computed by the Nudge Elastic Band method. Each successive exchange mechanism is characterized by Associative (A), Interchange Associative (I_A), Interchange Dissociative (I_D) or Dissociative (D) exchange, shown on each free energy surface. MD trajectory snapshots for each type of molecular unit with van der Waal's radius (colored surface) are depicted on top.

Fourier-transformed radial distribution function (RDF ΔG_{Cl}), shown in Fig. 1a, H(D)-bonding to chloride species (Cl^--H_w) is not seen because the D/^{nat}H isotopic ratio was matched to produce the null-scattering water solvent. The other Zn^{2+}-water or water-water structural correlations are also not seen because the only difference in scattering arising from $^{37}Cl/^{nat}Cl$ isotopes cancels all these contributions in the difference RDF ΔG_{Cl}. The advantage of using null-scattering water as a second isotope substitution is that it removes the Cl^--H_w hydrogen bonding signal at ~ 2.3 Å [47,48] and therefore eliminates the peak overlap that would interfere with the Zn^{2+}-Cl^- (~2.2 Å) contact ion-pair [31,48–50]. As shown in Fig. 1a, the observed ΔG_{Cl} (black curve) is simple enough that individual peaks can be readily identified, specifically the clear contact ion-pair signal for Zn^{2+}-Cl^- bonds at ~ 2.2 Å and another broad peak centered at ~ 3.7 Å that contains the Cl^--Cl^- intramolecular peaks for ion complexes containing multiple chlorides. The first-shell Cl^--O_w correlation at ~ 3.4 Å forms a shoulder on the Cl^--Cl^- peak.

To better understand the contributions of specific ion complexes to the experimental RDF peaks, the calculated RDFs derived from a 5 μs long (2 μs equilibration, 3 μs production) ECC-MD simulation (see Supplementary Material, Section S7) are plotted against the experimental data (Fig. 1a). Such a long equilibration time is required because of the slow solvent exchange of the aqueous zinc ions and zinc chloride complexes; see Supplementary Material, Figure S12 for a detailed plot of speciation of the system as a function of simulated time. To fit the experimental data, the Cl^--Cl^- and Zn^{2+}-O_w pair interactions from the published ECC force field [31] were modified to maximize the agreement in the intensities and radial distances of the Zn^{2+}-Cl^-, Cl^--Cl^-, and Cl^--O_w peaks between the experimental and theoretical results. As illustrated in Fig. 1a, the calculated total RDF ΔG_{Cl} (red dashed line and open circles) corresponds to Cl-NDIS data with three partial structure factors involved (i.e., atom–atom pair correlations of Cl^--O_w, Zn^{2+}-Cl^- and Cl^--Cl^-). There is overall good agreement in peak shapes for Zn^{2+}-Cl^- and Cl^--Cl^- peaks and the modified force field also fits literature Cl-NDIS (on 4.0 m $ZnCl_2$ in D_2O) data quite well (see Supplementary Material, Section S6). However, there are some portions of the fit to the data that could be improved, such as the Cl^--O_w shoulder is somewhat overestimated by the force field and the dip in scattering intensity at ~ 5 Å is not captured well. While its origin is not completely clear, the latter feature has been observed in previous chloride salt RDF experiments [51–54]. Regardless, the overall good agreement of the ECC-MD method and experiment makes the ECC-MD a useful tool to understand chemical speciation and reactivity in complex aqueous salt solu-

tions that can be considered to give a fairly accurate portrayal of the structure of the solution. To study these properties, we first decomposed the calculated RDF ΔG_{Cl} into the contributions from individual local ion complexes (shaded colored curves at the bottom of the plot in Fig. 1a). In our view, these extracted "speciation RDFs" centered around the metal-cations for the formation of ion-paired molecular moieties, $ZnCl_x(H_2O)_y^{2-x}$, are the most intuitive way to present a complex solution structural RDF, as compared to the traditional atom–atom pair correlations. This is because this method readily deconvolutes the total RDF into the contributions from the various molecular species that are present in the solution. Based on the geometry of the defined molecular species, the speciation RDF of, e.g., neutral-charged $ZnCl_2(H_2O)^0_{2\text{-}3}$ molecules (Fig. 1), contains two Zn^{2+}-Cl^- bonds (at ~ 2.2 Å), one Cl^--Cl^- (at ~ 3.8 Å), and various numbers of Cl^--O_w (at ~ 3.2 Å) intramolecular correlations. Note that in order to associate the primary intramolecular correlation for a given type of ion complex, the intermolecular interactions for the complex to the surrounding environment also need to be included in the speciation RDF calculation. In this way contributions from other solvation water about the Cl^- that are already ion-paired to Zn^{2+} can be considered (see Supplementary Material S5 for this method). Therefore, each speciation RDF shown in Fig. 1a represents not only the neutron-weighted contributions to the total observed ΔG_{Cl} intensity but also reflects the prevalent chemical ion complex species in 4.5 m $ZnCl_2$ solution.

The extracted coordination environments about the complexed Cl^- within the ECC-MD model and the agreement to the Cl-NDIS experimental data suggest that the structure of 4.5 m $ZnCl_2$ solution should be thought of as an assembled collection of ion complexes (or molecules that differ by the local specific bonded configurations), and the network of their molecular connectivity ultimately describes the dynamics and chemical reactivity in solution. Specifically, 12% of ion complex species are in the form of $Zn(H_2O)^{2+}_6$ (i.e., fully solvated Zn^{2+}), but the remaining 88% are bonded to 100% of the chlorine atoms, i.e., there is no free chloride observed, $Cl(H_2O)^-_{6\text{-}8}$. Among the zinc in ion pairs or complexes, average populations consist of approximately 10% $ZnCl(H_2O)^+_{4\text{-}5}$, 37% $ZnCl_2(H_2O)^0_{2\text{-}3}$, 32% $ZnCl_3(H_2O)^-_{1\text{-}2}$, with no observation of $ZnCl_4^{2-}$ species from direct simulation (see Supplementary Material, Figures S13 and S14 for the detailed distributions of species). A snapshot of the solution structure is displayed in Fig. 1b, in which the fully solvated state for each major type of the complexes is color-coded. What can be seen in this snapshot is that the ion complexes are in close proximity to each other but are usually separated by water molecules in solvent-separated configurations. A minority of chloride ions are found to be shared among multiple zinc atoms at this concentration, but they are limited to clusters containing only two zinc atoms, i.e., approximately 9% of species are of the form $Zn_2Cl_{3\text{-}5}(H_2O)^{+1,0}_{2\text{-}3}$. The neutron-weighted RDF contributions from these dimeric clusters are color-coded in purple in Fig. 1a, and the representative snapshot of these clusters is shown in Fig. 1b. This finding contrasts somewhat to some previous findings in calcium carbonate[5,8] where extended networks of ions directly bonded to each other have sometimes been found.

3.2. The stability of ion complexes and their reactivity

Beyond simple speciation, we can probe the reactivity of ion complexes in concentrated aqueous solutions and evaluate the strength of their interaction with the surrounding water molecules and other ion complexes. To accomplish this, we examined the coordination number of $n(Cl^-)$ and $n(O_w)$ around Zn^{2+} centers. We then used these two parameters as collective variables along our biased ECC-MD well-tempered metadynamics simulations to calculate the relative Helmholtz free energies, ΔA, of the ion complexes and a nudged elastic band method [46,55] to calculate a minimum free energy path (see Supplementary Material, Section S8). The coordination numbers $n(Cl^-)$ and $n(O_w)$ are defined as the number of Cl^- and O_w that are directly bonded to the Zn^{2+} center, and different molecular complexes $ZnCl_x(H_2O)_y^{2-x}$ can be distinguished (details are provided in Supplementary Material, Section S7). The derived free energy surface shown in Fig. 2a and the minimum energy pathway between states (dashed line) clearly indicate that, at a concentration of 4.5 m, there exist several stable and metastable coordination states. The two most stable coordination states, as indicated by the cooler temperature colors at the potential of mean force (PMF), are the tetrahedral molecules of $ZnCl_2(H_2O)^0_2$ and $ZnCl_3(H_2O)^-$ (referred to as (2,2) and (3,1) in the Figure), followed by penta-coordinated $ZnCl_2(H_2O)^0_3$ (2,3) species and octahedral molecule of $ZnCl(H_2O)^+_5$ (1,5) species. What is especially interesting in this plot is that the variability in water coordination numbers for a given number of chlorides in the ion complex. That is, while the aqueous zinc, $Zn(H_2O)^{2+}_6$, and fully saturated $ZnCl_4^{2-}$ are well-defined structures with fixed coordination numbers, all intermediate complexes can contain different numbers of water molecules for a given number of chlorides and these variations are often stable. The flexible coordination number of the intermediate species contrasts with the reactivity of dissolved aluminum [17] or magnesium [56,57] ions, where coordination number changes and solvent exchanges have been viewed as rate-controlling processes such as for dissolution and growth of solid phases [58]. If we follow the descriptions by Widmer *et al.* [59] for other electrolyte systems, the coordination states at each free energy minimum displayed in Figs. 2 and 3 with varying numbers of water molecules and chlorine ions should be thought of as distinct chemical (molecular) species, whose stabilities, local connectivity, and reaction pathways to the other species fundamentally control the solution-phase structure and chemical reactions. Using a Boltzmann distribution to obtain the speciation from the free energy surface gives a subtly different speciation than the direct simulation that is quoted above. Of specific note is that there is a wider array of species found in the biased simulation, and that the metadynamics-derived population suggested 2.7% of the zinc should be $ZnCl_4^{2-}$ species which was not observed in the direct simulation at all (see Supplementary Material, Figures S13 and S14 for comparison). The difference could be due to statistical sampling in the direct simulation, i.e., 2.7% of zinc species corresponds to ~ 4 zinc atoms in a simulation of 150 zinc total, which is a small number. Another possibility is that despite the direct simulation accounting for 5 μs of simulated time, it was perhaps not fully equilibrated for minor species that also have higher activation energies for their formation. A last possibility is that an unknown sampling error may in effect enhance the apparent stability of some species in the biased simulation. Regardless, the trends between biased and unbiased simulations are similar and differences on the order of a few percent can be viewed as random uncertainty in the true speciation of the simulations.

To ascertain the influence of the solvent molecules on reactivity and the effect of the close proximity of the ionic complexes to each other in concentrated solutions, we performed a "thought experiment" by comparing the free energy surface in 4.5 m $ZnCl_2$ to the same type of calculation for dilute conditions (0.01 m; Fig. 2b). In the dilute solution, the most stable state is clearly the fully solvated $Zn(H_2O)^{2+}_6$ (0,6) species and the free energy barriers to convert between species are noticeably smaller in dilute conditions than in concentrated solutions (Fig. 2). This means a shorter lifetime and dynamically faster reactions for the interconversions of different species in dilute solutions. The differences in the Helmholtz free energies for the two solutions are quantified in Fig. 3, in which the minimum energy pathways on the PMF surfaces in the two solutions are overlaid, with the free energies (ΔA) and free energy barriers to reaction ($\Delta A^{\ddagger}$) are shifted relative to the fully

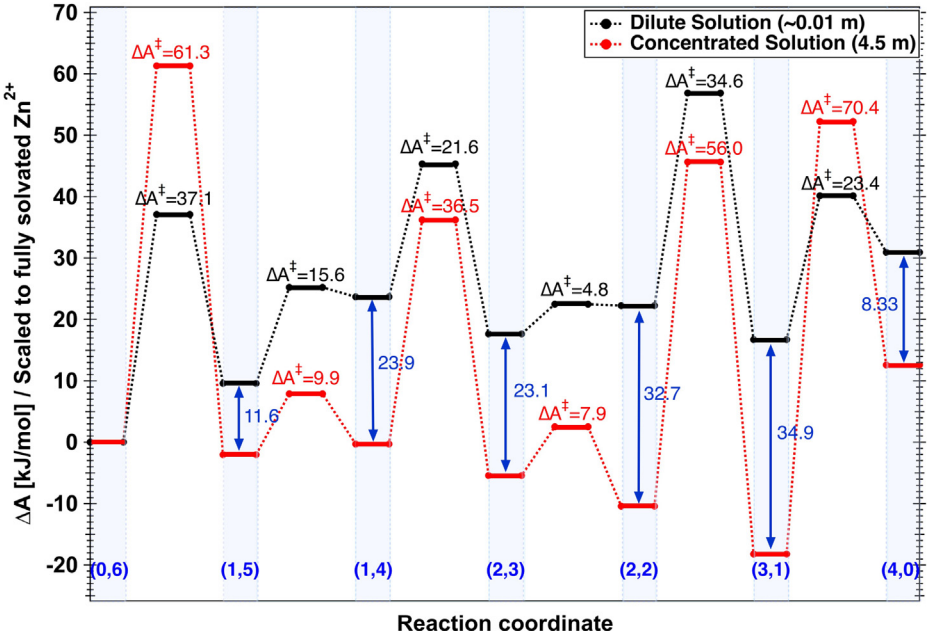

Fig. 3. Comparison of the minimum energy paths for concentrated (red) and dilute (black) solutions. The reaction coordinate is defined at the base (in bold blue), representing the Zn^{2+} coordination of each stable state ($n(Cl^-)$, $n(H_2O)$). Free energies are relative to the $Zn(H_2O)_6^{2+}$ coordination state in each solution (such that $\Delta A = 0$ for $Zn(H_2O)_6^{2+}$). Blue shaded portions show stable ion complexes separated by their respective free energy barriers ($\Delta A^{\ddagger}$), where the dotted lines illustrate the transition to each species. The blue arrows and text represent the difference in Helmholtz free energies of stable ion complexes in the concentrated and dilute solutions.

solvated $Zn(H_2O)_6^{2+}$ coordination state. The overall trend for ΔA in the concentrated solution is towards progressively more favorable free energies relative to $Zn(H_2O)_6^{2+}$, with the exception of forming the last species in the series, $ZnCl_4^{2-}$. However, the opposite trend is observed in the dilute solution, where increasing numbers of bound chlorides becomes less energetically favorable. Despite the increased thermodynamic favorability of complex formation in the concentrated solution, however, there is a significant increase in the free energy barriers to reaction ($\Delta A^{\ddagger}$) relative to the dilute solution. Particularly large $\Delta A^{\ddagger}$ conversions are between Zn $(H_2O)_6^{2+}$ (0,6) ↔ $ZnCl(H_2O)_5^{+}$ (1,5), $ZnCl_2(H_2O)_2^{0}$ (2,2) ↔ $ZnCl_3(H_2O)^-$ (3,1), and $ZnCl_3(H_2O)^-$ (3,1) ↔ $ZnCl_4^{2-}$ (4,0) species (Fig. 3). The interconversions of the species in the concentrated solution nearly uniformly display a higher activation free energy in concentrated relative to dilute solution (as high as an increase of 47 kJ/mol in the case of $ZnCl_3(H_2O)^-$ to $ZnCl_4^{2-}$). The implications are that it is more thermodynamically favorable to form ion complexes in the concentrated solution, but the kinetics of complex formation and dynamics of ligand exchange are expected to slow down dramatically at the same time.

Beyond just the free energies, the minimum energy path (Fig. 2) also reveals the reaction mechanism for breaking bonds from the leaving water molecules and forming bonds to the entering anions (or vice versa for dissociation of the ion complex). The pathways from the well-tempered metadynamics are supported by individual observations of individual ligand exchange events during direct simulation [60] (see Supplementary Material, Section S8). We classify the reaction mechanisms in the two salt solutions according to the Langford-Grey ligand substitution reactions [16]. Differences include, firstly, the (0,6) ↔ (1,5) interconversion reaction is a dissociative (D) type in dilute conditions but contains a more interchange dissociative (I_D) character at 4.5 m concentration (Fig. 2). The difference between these mechanisms is that during a dissociative exchange mechanism, the $Zn(H_2O)_6^{2+}$ (0,6) complex loses a single coordinating water molecule first, forming an intermediate metastable species with decreased coordination number, i.e., a (0,5) species (Fig. 2b), followed by gaining a chloride to form the $ZnCl(H_2O)_5^{+}$ (1,5) species. The interchange dissociative mechanism (I_D) does not have a discernible intermediate of lower coordination number formed, in comparison, because the leaving and entering ligands exchange simultaneously without forming a metastable intermediate. The mechanism is further characterized as interchange dissociative (I_D) rather than simple dissociative because the ligands contain somewhat longer distances than their equilibrium lengths when they exchange. In contrast to the initial zinc chloride ion pair formation, the (3,1) ↔ (4,0) reaction is found to have an I_D mechanism character in both dilute and concentrated conditions (Fig. 2). The (2,2) ↔ (3,1) reaction is also an I_D mechanism in dilute solution but switches at 4.5 m to a mixed character of associative (A)/interchange associative (I_A) mechanism (Fig. 2). For an A/I_A mechanism of the (2,2) ↔ (3,1) reaction, there is an increase in the coordination of the complex (bond making) and a formation of metastable penta-coordinated (3,2) species, which then converts to the more stable (3,1) species (Fig. 2a). The interconversion reaction in the (1,5) ↔ (2,2) process is perhaps the most interesting one because the reaction requires a change of total coordination of the zinc ion from octahedral to tetrahedral geometry (or reverse). At the elevated concentration, the process evidently involves two separate desolvation (or solvation in reverse) steps with I_A type mechanism for chlorination in between (Fig. 2). This results in the formation of relatively stable (1,4) and (2,3) penta-coordinated compounds with small energy barriers for (1,5) ↔ (1,4) and (2,3) ↔ (2,2) reactions, respectively (Fig. 3). This observation suggests that the persistence of the penta-coordinated species is important for the kinetic conversion between octahedral and tetrahedral molecular entities at concentrated $ZnCl_2$ solution. A similar penta-coordinate species has been observed for aluminum, with the difference that the aluminum requires deprotonation of one of the first shell waters to form a penta-coordinate complex(14), whereas here there are multiple stable penta-coordinate intermediate ion complexes that form, (1,4) and (2,3), during the course of forming higher-order ion complexes. Overall, however, we found that, beyond just the thermodynamics and the activation free energies for complex formation,

the reaction mechanism itself is also strongly affected by the solute/solution structure and its surrounding environment in complex aqueous solutions.

3.3. Thermodynamic association constants for complex formation.

As can be deduced from Figs. 2 and 3, the increased stability of molecular compounds at elevated concentrations also changes the thermodynamic association constants for complex formation (K_A). In the reaction expressions given in Table 2, log K_A reflects the affinity of a Cl^- ligand to a particular type of $ZnCl_x^{2-x}$ complex (x = 0–4). To compare to literature data, we ignore the number of solvation waters in the ion complexes here.

Four K_A values were extracted from a separate series of one-dimensional well-tempered metadynamics simulations that used Zn^{2+}-Cl^- distance as a reaction coordinate, and equilibrium constants were calculated after integration of the Boltzmann distribution, following previous practice [61–63] (see Supplementary Material, Section S9). It is readily apparent in Table 2 that the calculated association constants change with respect to the concentration of the solution (i.e., 0.01 m vs. 4.5 m). The formation of mono- and dichloride species is more than an order of magnitude more favorable in the concentrated solution relative to the dilute one, while formation of tri- and tetrachloride species is enhanced in the concentrated solution by almost a factor of four. In both concentrations, the formation constants for $ZnCl_2^0$ and $ZnCl_3^-$ are larger and more positive, whereas $ZnCl^+$ and $ZnCl_4^{2-}$ are less favorable. This is consistent with the relative intensities of the Cl^--Cl^- and Cl^--O_w peaks in the NDIS shown in Fig. 1a, which indicate that a majority of species include more than one chloride (and if anything, the ECC-MD underestimates the average number of chlorides in the ion complexes relative to the NDIS results). Our findings contrast with the available literature equilibrium constants where typically $ZnCl^+$ or $ZnCl_2$ are found to be the most common ion complex. Other multi-chloride ion complexes are either found to be less favorable, or not included in the fit at all (Table 2).

An important question is to identify the phenomena responsible for the concentration-dependent changes in the thermodynamic stability, reactivity and mechanisms. We hypothesize that the molecular basis for the observed changes in concentrated salt solution should arise from the short-range interactions and adjustment of solvation environments around the formed complex entities in the solution. As the dissolved salt concentration increases, the complete hydration shell morphology could be perturbed by introducing competition for solvent molecules. The adjustments of an ion complex to its local surrounding environment in response to this competition would thus be reflected in thermodynamic stability changes at increased concentrations. To test this hypothesis, in Fig. 4, we calculated various atom–atom RDFs for different ion complexes by sampling the trajectories of the biased ECC-MD simulations to find representative complexes in the local minima and running a new short-term unbiased simulation starting with those configurations. What is observed is that in the concentrated solutions, there are abundant solute species in the second and third shells of each of the complexes of a given type that are missing in the dilute solution. Particularly notice the first Zn^{2+}-Zn^{2+} peak, nearly constant and clearly present even for positively charged clusters a,b, while the first Zn^{2+}-Cl^- peak decreases as the complex becomes negatively charged. Thus, it is clear that the solution structure at the high concentration changes the solvation environment of the ion complexes. The change in extended solvation environment should therefore also be responsible for the observed changes in thermodynamic stability of complexes, the increased free energies of activation for interconversion of species, and shift towards more associative reaction mechanisms for (2,2) ↔ (3,1) complexation reaction in concentrated solutions.

3.4. Perspectives on the structure of ion complexes and their correlation to solid compounds

One aspect that is not captured in the above discussion thus far is the propensity to form larger-scale ion clusters in the concentrated solution. As noted above, in Fig. 1, we find that 9% of species contain more than one zinc atom (referred to as multimers), and well-tempered metadynamics simulations utilizing a zinc-zinc coordination number as a collective variable confirmed similar amounts (See Supplementary Material, Section S10). The composition of these multimers is restricted to species of the form $Zn_2Cl_{3-5}(H_2O)_{2\text{-}3}^{0,1\pm}$ (where charge varies with the number of chlorines in the complex). While these multi-zinc species are a minority at 4.5 m, it is not clear if their population and composition will change at even higher concentrations (solubility of $ZnCl_2$ is on the order of ~ 30 m at 25 °C [66]). However, we can compare these species to the crystal structures of zinc chloride compounds, with the goal of determining if these are plausible precursors to the nucleation of solid products. Firstly, in the anhydrous $ZnCl_2$ polymorphs (α, β, γ, and δ), all the Zn^{2+} cations are tetrahedrally coordinated to four Cl^- anions and are all corner-shared to form a $ZnCl_4^{2-}$ framework structure. $ZnCl_4^{2-}$ is a minority species at 4.5 m with only 2.7% predicted by the biased simulations. Given these two observations, one would consider that formation of zinc multimers in solution are plausible precursors for nucleation of anhydrous $ZnCl_2$ solids, especially since only the anhydrous phase is stable above 28 °C [67]. At lower temperatures, hydrate crystals of $ZnCl_2 \bullet R(H_2O)$ (with R = 1.33, 2.5, 3, 4, and 4.5) form [68]. For these, the 1.33-hydrate solid is stable at room temperature and consists of chains of $ZnCl_4^{2-}$ that are linked by a few octahedral $ZnCl_2(H_2O)_4^0$ units whose Cl^- are shared and bridge the chains [69]. The coordination structure of 2.5-hydrate is composed of an isolated $Zn_2Cl_4(H_2O)_5^0$ complex made from an octahedral $ZnCl(H_2O)_5^+$ unit with the Cl^- anion also shared with a tetrahedral $ZnCl_4^{2-}$ unit. These two hydrous compounds and anhydrous $ZnCl_2$ structures support the idea that the packing of monomeric complexes into bi-molecular ion clusters or multimers are plausible precursors for the nucleation of the bulk structures. In contrast, the structures of the 3- and 4.5-hydrates consist solely of the isolated molecular units of $Zn(H_2O)_6^{2+}$ octahedra and $ZnCl_4^{2-}$ tetrahedra, i.e., no multimers are present. Therefore, it is not likely that increased polymerization leads to nucleation of

Table 2
Association constants (K_A) for complex formation calculated at 0.01 and 4.5 m, compared to those of a range of literature data.

Reaction	log K_A					
	0.01 m*	4.5 m*	0.1–1.0 m[28]	0.1–3.0 m[30,32]	~0.1–1.5 m[33,34,64]	0.1–3.7 m [65]
$Zn^{2+} + Cl^- \longleftrightarrow ZnCl^+$	−0.67	+0.69	+0.20	+0.43	−0.19	+0.49
$ZnCl^+ + Cl^- \longleftrightarrow ZnCl_2^0$	+0.49	+1.50	+0.05	+0.18	+0.18	+0.62
$ZnCl_2^0 + Cl^- \longleftrightarrow ZnCl_3^-$	+0.68	+1.25	n.f.	−0.08	−1.4	+0.10
$ZnCl_3^- + Cl^- \longleftrightarrow ZnCl_4^{2-}$	−2.47	−1.91	n.f.	−0.33	−1.52	−0.51

n.f. = not included in fit due to lack of data * This work.

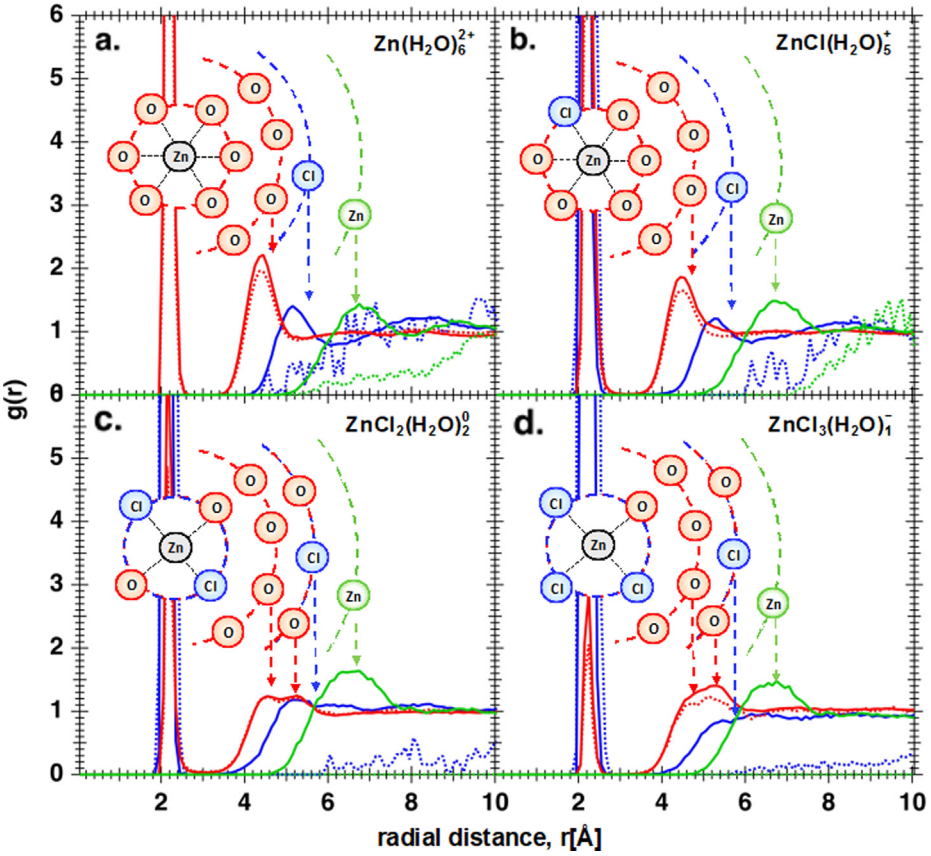

Fig. 4. Atom-Atom radial distribution functions and schematics of extended solvation structures for selected ion complexes. Radial probabilities (g(r)) as a function of distance from the zinc ion for (a) $Zn(H_2O)_6^{2+}$ (b) $ZnCl(H_2O)_5^+$ (c) $ZnCl_2(H_2O)_2^0$ and (d) $ZnCl_3(H_2O)_1^-$ are extracted by running independent short-term, unbiased simulations that start from species configurations harvested from minima in Fig. 2. Dashed lines represent those species in dilute solution (0.01 m) and solid lines represent concentrated solution (4.5 m). The extended solvation structures of the ion complexes are illustrated using schematics using color circles for the locations of chlorine (blue), zinc (green) and oxygen on water (red) with respect to the central zinc atom (black). Arrows correspond to the location of each species in the g(r).

these phases. Interestingly, the formation pattern displayed here, that of less highly-polymerized structures at increasingly lower temperatures, is the opposite of that of silicate phases where increasing temperatures favor less highly-polymerized structures.

In the 4.5 m solution, however, the two most stable coordinated compounds are $ZnCl_3(H_2O)_{1\text{-}2}^-$ and neutral $ZnCl_2(H_2O)_{2\text{-}3}^0$ complexes, not multimeric species. Since we observed an increased activitation energy barrier for formation of higher order ion complexes relative to the dilute solution, we hypothesize that the extended solvation structure in concentrated solutions acts as a source of frustration that works against polymerization and formation of crystallization precursors, such as pre-nucleation clusters [1,2,5,7]. Similar arguments have been applied to explain the high glass-forming ability of lithium chloride (LiCl) solutions [70,71] and the high stability of supersaturated sodium thiosulfate ($Na_2S_2O_3$) aqueous solutions [72]. In the LiCl case, it has been suggested that the competition between short-range or local molecular structures (such as found here) vs. long-range structure or global bond ordering (to form a stable crystal) in an aqueous system allows it to bypass crystallization and vitrify upon cooling [70,71]. In the $Na_2S_2O_3$ solutions, the presence of geometrically frustrated clusters with long lifetimes prevents the formation of the thermodynamically stable crystalline state [72]. Furthermore, broader recognition of metal–ligand complex formation and constituent character in aqueous solutions could allow us to develop new strategies in chemical synthesis with targeted structures or reaction rates, such as, introducing different or competing counterions to tailor the preferred extended solvation structure of molecular complexes or solute entities that control or promote crystallization processes and their kinetics [73–75] by manipulating extended solvation structures.

4. Conclusions

Overall, we revealed in this work that the extended solvation environment and molecular connectivity of a concentrated $ZnCl_2$ aqueous salt solution strongly influences the thermodynamic stability, kinetics and reaction mechanism for formation of ion complexes. This suggests that equilibrium "constants" reported for this and other concentrated aqueous systems may be, in fact, dependent on the solute concentration at which they are measured. The ion complexes that form in the concentrated solution are separated by solvent molecules for the most part. This contrasts to some networks previously reported where extensive direct bonds between ions are found. In addition, the networks of solvated ion complexes found in this complex solution also seemingly inhibit nucleation of crystalline phases by increasing the energy barriers to conversion between species. These findings expand the current understanding of precipitating solids that direct crystal nucleation, in that it suggests that specific solute constituents compatible to the solid structure need to be present in solution to facilitate their interaction for crystallization. A further implication of this work is that the concentration-dependent effects observed here are significant in complex solutions and perhaps even ubiquitous throughout solution chemistry, albeit with

high variability between different systems and species. These extended solvation structure effects are not accounted for in typical classical non-ideality corrections, such as activity-concentration effects.

CRediT authorship contribution statement

Nikhil Rampal: Methodology, Software, Writing - review & editing. **Hsiu-Wen Wang:** Investigation, Supervision, Formal analysis, Writing - review & editing. **Denys Biriukov:** Methodology, Software, Writing - review & editing. **Alexander B. Brady:** Methodology. **Joerg C. Neuefeind:** Investigation, Formal analysis, Resources. **Milan Předota:** Supervision, Writing - review & editing, Project administration, Funding acquisition. **Andrew G. Stack:** Conceptualization, Investigation, Writing - review & editing, Project administration, Funding acquisition, Supervision.

Declaration of Competing Interest

The authors declare that they have no known competing financial interests or personal relationships that could have appeared to influence the work reported in this paper.

Acknowledgments

This material is primarily based upon work supported by the U. S. Department of Energy, Office of Science, Office of Basic Energy Sciences, Chemical Sciences, Geosciences, and Biosciences Division. The research at the Spallation Neutron Source at Oak Ridge National Laboratory, was supported by the Scientific User Facilitates Division, BES, DOE. D.B. and M.P. were supported by the Ministry of Education, Youth, and Sports of the Czech Republic, project LTAUSA17163.

Appendix A. Supplementary data

Supplementary data to this article can be found online at https://doi.org/10.1016/j.molliq.2021.116898.

References

[1] K. Henzler, E.O. Fetisov, M. Galib, M.D. Baer, B.A. Legg, C. Borca, J.M. Xto, S. Pin, J.L. Fulton, G.K. Schenter, Supersaturated calcium carbonate solutions are classical, Sci. Adv. 4 (2018) eaao6283.
[2] D. Gebauer, P. Raiteri, J.D. Gale, H. Colfen, On Classical and Non-Classical Views on Nucleation, Am. J. Sci. 318 (2018) 969.
[3] G.C. Sosso, J. Chen, S.J. Cox, M. Fitzner, P. Pedevilla, A. Zen, A. Michaelides, Crystal nucleation in liquids: Open questions and future challenges in molecular dynamics simulations, Chem. Rev. 116 (2016) 7078.
[4] A.S. Myerson, B.L. Trout, Nucleation from solution, Science 341 (2013) 855.
[5] A.F. Wallace, L.O. Hedges, A. Fernandez-Martinez, P. Raiteri, J.D. Gale, G.A. Waychunas, S. Whitelam, J.F. Banfield, J.J. De Yoreo, Microscopic evidence for liquid-liquid separation in supersaturated $CaCO_3$ solutions, Science 341 (2013) 885.
[6] D. Gebauer, A. Volkel, H. Colfen, Stable Prenucleation Calcium Carbonate Clusters, Science 322 (2008) 1819.
[7] D. Gebauer, H. Colfen, Prenucleation clusters and non-classical nucleation, Nano Today 6 (2011) 564.
[8] R. Demichelis, P. Raiteri, J.D. Gale, D. Quigley, D. Gebauer, Stable prenucleation mineral clusters are liquid-like ionic polymers, Nat. Commun. 2 (2011).
[9] D. Genovese, M. Montalti, F. Otalora, J. Gomez-Morales, M. Sancho-Tomas, G. Falini, J.M. Garcia-Ruiz, Role of $CaCO_3$ degrees Neutral Pair in Calcium Carbonate Crystallization, Cryst. Growth Des. 16 (2016) 4173.
[10] P.J.M. Smeets, A.R. Finney, W.J.E.M. Habraken, F. Nudelman, H. Friedrich, J. Laven, J.J. De Yoreo, P.M. Rodger, N.A.J.M. Sommerdijk, A classical view on nonclassical nucleation, P. Natl. Acad. Sci. USA 114 (2017) E7882.
[11] A. Carino, A. Testino, M.R. Andalibi, F. Pilger, P. Bowen, C. Ludwig, Thermodynamic-kinetic precipitation modeling. A case study: The amorphous calcium carbonate (ACC) precipitation pathway unravelled, Cryst. Growth Des. 17 (2017) 2006.
[12] A.R. Felmy, D. Rai, J.E. Amonette, The Solubility of Barite and Celestite in Sodium-Sulfate - Evaluation of Thermodynamic Data, J. Solution Chem. 19 (1990) 175.
[13] A.R. Felmy, D. Rai, R.W. Fulton, The Solubility of AmOHCO3 (c) and the Aqueous Thermodynamics of the System Na+-Am 3+-HCO3–CO32–OH–H2O, Radiochim. Acta 50 (1990) 193.
[14] L.N. Plummer, E. Busenberg, The solubilities of calcite, aragonite and vaterite in CO_2-H_2O solutions between 0 and 90 C, and an evaluation of the aqueous model for the system $CaCO_3$-CO_2-H_2O, Geochim. Cosmochim. Ac. 46 (1982) 1011.
[15] J.R. Rustad, W.H. Casey, Metastable structures and isotope exchange reactions in polyoxometalate ions provide a molecular view of oxide dissolution, Nat. Mater. 11 (2012) 223.
[16] C.H.G. Langford, H. B., Ligand Substitution Processes. W. A. Benjamin, 1966.
[17] T.W. Swaddle, J. Rosenqvist, P. Yu, E. Bylaska, B.L. Philiips, W.H. Casey, Kinetic evidence for five-coordination in $AlOH(aq)^{2+}$ ion, Science 308 (2005) 1450.
[18] S. Roy, M.D. Baer, C.J. Mundy, G.K. Schenter, Marcus Theory of Ion-Pairing, J. Chem. Theory Comput. 13 (2017) 3470.
[19] D.T. Richens, Ligand substitution reactions at inorganic centers, Chem. Rev. 105 (2005) 1961.
[20] J. Aqvist, Ion Water Interaction Potentials Derived from Free-Energy Perturbation Simulations, J. Phys. Chem. 94 (1990) 8021.
[21] L.X. Dang, J.E. Rice, P.A. Kollman, The Effect of Water Models on the Interaction of the Sodium-Chloride Ion-Pair in Water - Molecular-Dynamics Simulations, J. Chem. Phys. 93 (1990) 7528.
[22] J.P. Larentzos, L.J. Criscenti, A Molecular Dynamics Study of Alkaline Earth Metal-Chloride Complexation in Aqueous Solution, J. Phys. Chem. B 112 (2008) 14243.
[23] H.W. Wang, L. Vlcek, J.C. Neuefeind, K. Page, S. Irle, J.M. Simonson, A.G. Stack, Decoding Oxyanion Aqueous Solvation Structure: A Potassium Nitrate Example at Saturation, J. Phys. Chem. B 122 (2018) 7584.
[24] D. Semrouni, H.-W. Wang, S.B. Clark, C.I. Pearce, K. Page, G. Schenter, D.J. Wesolowski, A.G. Stack, A.E. Clark, Resolving local configurational contributions to X-ray and neutron radial distribution functions within solutions of concentrated electrolytes–a case study of concentrated NaOH, PCCP 21 (2019) 6828.
[25] L. Helm, A.E. Merbach, Water exchange on metal ions: experiments and simulations, Coordin. Chem. Rev. 187 (1999) 151.
[26] A. Barducci, M. Bonomi, M. Parrinello, Metadynamics, WIREs Comput. Mol. Sci. 1 (2011) 826.
[27] A. Laio, M. Parrinello, Escaping free-energy minima, P. Natl. Acad. Sci. USA 99 (2002) 12562.
[28] H.C. Helgeson, Thermodynamics of hydrothermal systems at elevated temperatures and pressures, Am. J. Sci. 267 (1969) 729.
[29] E.L. Shock, H.C. Helgeson, D.A. Sverjensky, Calculation of the Thermodynamic and Transport-Properties of Aqueous Species at High-Pressures and Temperatures - Standard Partial Molal Properties of Inorganic Neutral Species, Geochim. Cosmochim. Acta 53 (1989) 2157.
[30] D.A. Sverjensky, E.L. Shock, H.C. Helgeson, Prediction of the thermodynamic properties of aqueous metal complexes to 1000 degrees C and 5 kb, Geochim. Cosmochim. Acta 61 (1997) 1359.
[31] E. Duboue-Dijon, P.E. Mason, H.E. Fischer, P. Jungwirth, Hydration and Ion Pairing in Aqueous Mg^{2+} and Zn^{2+} Solutions: Force-Field Description Aided by Neutron Scattering Experiments and Ab Initio Molecular Dynamics Simulations, J. Phys. Chem. B 122 (2018) 3296.
[32] S.A.W. Daveler, T. J., EQPT, A Data File Preprocessor for the EQ3/6 Software Package: User's Guide and Related Documentation (Version 7.0), (1992).
[33] F. Zhu, D. Persson, D. Thierry, C. Taxen, Formation of corrosion products on open and confined zinc surfaces exposed to periodic wet/dry conditions, Corrosion 56 (2000) 1256.
[34] L.G. Sillén, A.E. Martell, J. Bjerrum, Stability constants of metal-ion complexes, Chemical Society, London, 1964.
[35] H. Tialowska-Mocharla, S. Manohar, G. Atkinson, Activity coefficient measurements of the system $HCl-ZnCl_2-H_2O$ at 25 and 35°C, J. Solution Chem. 21 (1992) 545.
[36] J. Neuefeind, M. Feygenson, J. Carruth, R. Hoffmann, K.K. Chipley, The Nanoscale Ordered MAterials Diffractometer NOMAD at the Spallation Neutron Source SNS, Nucl. Instrum. Meth. B. 287 (2012) 68.
[37] S. Plimpton, Computational Limits of Classical Molecular-Dynamics Simulations, Comp. Mater. Sci. 4 (1995) 361.
[38] S. Plimpton, Fast Parallel Algorithms for Short-Range Molecular-Dynamics, J. Comput. Phys. 117 (1995) 1.
[39] H. Bekker, H.J.C. Berendsen, E.J. Dijkstra, S. Achterop, R. Vondrumen, D. Vanderspoel, A. Sijbers, H. Keegstra, B. Reitsma, M.K.R. Renardus, Gromacs - a Parallel Computer for Molecular-Dynamics Simulations, Phy, Comp. (1993) 252.
[40] H.J.C. Berendsen, D. Vanderspoel, R. Vandrunen, Gromacs - a Message-Passing Parallel Molecular-Dynamics Implementation, Comput. Phys. Commun. 91 (1995) 43.
[41] D. Van der Spoel, E. Lindahl, B. Hess, G. Groenhof, A.E. Mark, H.J.C. Berendsen, GROMACS: Fast, flexible, and free, J. Comput. Chem. 26 (2005) 1701.
[42] S. Melchionna, G. Ciccotti, B.L. Holian, Hoover Npt Dynamics for Systems Varying in Shape and Size, Mol. Phys. 78 (1993) 533.
[43] L. Martinez, R. Andrade, E.G. Birgin, J.M. Martinez, PACKMOL: A Package for Building Initial Configurations for Molecular Dynamics Simulations, J. Comput. Chem. 30 (2009) 2157.
[44] I. Leontyev, A. Stuchebrukhov, Accounting for electronic polarization in non-polarizable force fields, PCCP 13 (2011) 2613.

[45] G.A. Tribello, M. Bonomi, D. Branduardi, C. Camilloni, G. Bussi, PLUMED 2: New feathers for an old bird, Comput. Phys. Commun. 185 (2014) 604.
[46] P. Hošek, V. Spiwok, Metadyn View: Fast web-based viewer of free energy surfaces calculated by metadynamics, Comput. Phys. Commun. 198 (2016) 222.
[47] S.J. Stuart, B. Berne, Effects of polarizability on the hydration of the chloride ion, J. Phys. Chem. 100 (1996) 11934.
[48] D.H. Powell, P.M.N. Gullidge, G.W. Neilson, M.C. Bellissentfunel, Zn^{2+} Hydration and Complexation in Aqueous-Electrolyte Solutions, Mol. Phys. 71 (1990) 1107.
[49] M. Maeda, T. Ito, M. Hori, G. Johansson, The structure of zinc chloride complexes in aqueous solution, Zeitschrift für Naturforschung A 51 (1996) 63.
[50] A. Zeidler, P.S. Salmon, R.A. Martin, T. Usuki, P.E. Mason, G.J. Cuello, S. Kohara, H.E. Fischer, Structure of liquid and glassy $ZnCl_2$, Phys. Rev. B. 82 (2010) 104208.
[51] D.H. Powell, A.C. Barnes, J.E. Enderby, G.W. Neilson, P.S. Salmon, The hydration structure around chloride ions in aqueous solution, Faraday Discuss. Chem. Soc. 85 (1988) 137.
[52] S. Cummings, J.E. Enderby, R.A. Howe, Ion Hydration in Aqueous $CaCl_2$ Solutions, J. Phys. C. Solid State 13 (1980) 1.
[53] P.S. Salmon, G. Neilson, J. Enderby, The structure of Cu^{2+} aqueous solutions, J. Phys. C. Solid State 21 (1988) 1335.
[54] J. Wilson, S. Ansell, J. Enderby, G. Neilson, Water structure around chloride ions in the presence of biological macromolecules, Chem. Phy. Lett. 278 (1997) 21.
[55] G. Henkelman, H. Jónsson, Improved tangent estimate in the nudged elastic band method for finding minimum energy paths and saddle points, J. Chem. Phys. 113 (2000) 9978.
[56] A. Mucci, J.W. Morse, The incorporation of Mg^{2+} and Sr^{2+} into calcite overgrowths: influences of growth rate and solution composition, Geochim. Cosmochim. Ac. 47 (1983) 217.
[57] F. Lippmann, Sedimentary Carbonate Minerals, Springer (1973) 5–96.
[58] Z. Shen, S.N. Kerisit, A.G. Stack, K.M. Rosso, Free-energy Landscape of the Dissolution of Gibbsite at High pH, J. Phys. Chem. Lett. 9 (2018) 1809.
[59] D.R. Widmer, B.J. Schwartz, Solvents can control solute molecular identity, Nat. Chem. 10 (2018) 910.
[60] A.G. Stack, J.R. Rustad, W.H. Casey, Modeling water exchange on an aluminum polyoxocation, J. Phys. Chem. B 109 (2005) 23771.
[61] P. Raiteri, R. Demichelis, J.D. Gale, Thermodynamically Consistent Force Field for Molecular Dynamics Simulations of Alkaline-Earth Carbonates and Their Aqueous Speciation, J. Phys. Chem. C 119 (2015) 24447.
[62] J.R. Rustad, A.G. Stack, Molecular dynamics calculation of the activation volume for water exchange on Li, J. Am. Chem. Soc. 128 (2006) 14778.
[63] R. Rey, E. Guardia, Dynamic Aspects of the Na^{+}-Cl^{-} Ion-Pair Association in Water, J. Phys. Chem. 96 (1992) 4712.
[64] G. Scibona, F. Orlandini, P. Danesi, Extraction of zinc chloride from aqueous chloride solutions by hydrocarbon solutions of quaternary ammonium chloride salt Attempt to evaluate the zinc chloride complexes by means of the extraction data, J. Inorg. Nucl. Chem. 28 (1966) 1313.
[65] Y. Mei, D. M. Sherman, W. Liu, B. Etschmann, D. Testemale, J. Brugger, Zinc complexation in chloride-rich hydrothermal fluids (25–600 °C): A thermodynamic model derived from ab initio molecular dynamics. Geochim. Cosmochim. Acta, 150, 265-284.
[66] W. Haynes, CRC Handbook of Chemistry and Physics, CRC Press, 2014.
[67] B. Aylett, Group IIB, Pergamon Press, 1973.
[68] J.W. Mellor, A comprehensive treatise on inorganic and theoretical chemistry. Longmans, Green and Company, 1923.
[69] v.H. Follner, B. Brehler, Die Kristallstruktur des ZnCl2. 4/3H2O, Acta. Crystallogr. B. 26 (1970) 1679.
[70] M. Kobayashi, H. Tanaka, Possible Link of the V-Shaped Phase Diagram to the Glass-Forming Ability and Fragility in a Water-Salt Mixture, Phys. Rev. Lett. 106 (2011).
[71] M. Kobayashi, H. Tanaka, Relationship between the phase diagram, the glass-forming ability, and the fragility of a water/salt mixture, J. Phys. Chem. B 115 (2011) 14077.
[72] J. Reichenbach, K. Wynne, Frustration vs prenucleation: Understanding the surprising stability of supersaturated sodium thiosulfate solutions, J. Phys. Chem. B 122 (2018) 7590.
[73] G.B. Jin, J. Lin, S.L. Estes, S. Skanthakumar, L. Soderholm, Influence of countercation hydration enthalpies on the formation of molecular complexes: a Thorium–nitrate example, J. Am. Chem. Soc. 139 (2017) 18003.
[74] D. Gebauer, S.E. Wolf, Designing solid materials from their solute state: a shift in paradigms toward a holistic approach in functional materials chemistry, J. Am. Chem. Soc. 141 (2019) 4490.
[75] H.W. Wang, T.R. Graham, E. Mamontov, K. Page, A.G. Stack, C.I. Pearce, Countercations Control Local Specific Bonding Interactions and Nucleation Mechanisms in Concentrated Water-in-Salt Solutions, J. Phys. Chem. Lett. 10 (2019) 3318.